A method to determine the acoustic reflection and absorption coefficients of porous media by using modal dispersion in a waveguide

Jevgenija Prisutova[a] and Kirill Horoshenkov
Department of Mechanical Engineering, University of Sheffield, Sheffield, S1 3JD, United Kingdom

Jean-Philippe Groby and Bruno Brouard
Laboratoire d'Acoustique de l'Université du Maine, UMR6613 CNRS/Univ. du Maine, F-72085 Le Mans Cedex 9, France

(Received 31 January 2014; revised 16 October 2014; accepted 17 October 2014)

The measurement of acoustic material characteristics using a standard impedance tube method is generally limited to the plane wave regime below the tube cut-on frequency. This implies that the size of the tube and, consequently, the size of the material specimen must remain smaller than a half of the wavelength. This paper presents a method that enables the extension of the frequency range beyond the plane wave regime by at least a factor of 3, so that the size of the material specimen can be much larger than the wavelength. The proposed method is based on measuring of the sound pressure at different axial locations and applying the spatial Fourier transform. A normal mode decomposition approach is used together with an optimization algorithm to minimize the discrepancy between the measured and predicted sound pressure spectra. This allows the frequency and angle dependent reflection and absorption coefficients of the material specimen to be calculated in an extended frequency range. The method has been tested successfully on samples of melamine foam and wood fiber. The measured data are in close agreement with the predictions by the equivalent fluid model for the acoustical properties of porous media.
 [http://dx.doi.org/10.1121/1.4900598]

PACS number(s): 43.20.Mv, 43.20.Ye, 43.55.Ev, 43.58.Bh [MV] Pages: 2947–2958

I. INTRODUCTION

Impedance tube measurements are used extensively for acoustic material characterization. The procedure for the determination of the plane wave, normal incidence acoustic absorption coefficient of a material is detailed in ISO 10534-2.[1] However, the high frequency limit for this regime is restricted by the diameter of a circular tube, d, or the side length of a square cross-section tube. In this case, the standard requirement is that the minimum wavelength, λ, at which the measurement procedure works is $\lambda > 1.72d$ (or $\lambda > 2d$ when the impedance tube is of a square cross-section of side d). As a result, there is often a conflict between the high frequency limit which needs to be achieved and the size of the samples which the tube is able to accommodate in order to determine the acoustical absorbing properties for a representative area of the material specimen. Several efforts have been made in the past to overcome this problem. Coulon *et al*. used an impedance tube coupled with a horn[2] to increase the area of the sample which can be tested under the plane wave regime. This method is believed to work well provided there is little or no scattering of the incident plant wave into higher order modes. Akoum and Ville[3] and Schultz *et al*.[4] have been the first to propose multi-modal decomposition methods which can be used to extend the frequency range of an impedance tube to enable to measure the reflection and absorption properties of relatively large material specimens beyond the maximum frequency of the plane wave regime in an acoustic waveguide. However, these works are based on the use of a number of microphone pairs installed at several cross-sectional positions near the terminated end of the waveguide. It can be argued that the use of several microphones increases the probability of a phase mismatch and can be time-consuming in terms of calibration. Additionally, the proximity of these microphones to the acoustic termination can result in a poor signal-to-noise ratio, problems associated with the standing waves in the tube and with the influence of the evanescent modes near the tube termination. Out-of-tube methods of the reflection and absorption measurements at oblique incidence also exist, as it was detailed by Tamura.[5,6] In these papers, the numerical method to measure the reflection coefficient at the range of angles is described and its predictions are compared to experimentally obtained results for two types of material. One can assume the theoretical underpinning of the Tamura's method enables us to suggest that this method can be more stable than the one described in this paper, as it does not employ numerical fitting and function minimization. However, the method by Tamura predicts the total reflection coefficient instead of modal reflection coefficient, which might be of interest in some cases. The experimental setup detailed in Tamura's paper is also not easy to run, as it requires an anechoic chamber to control the unwanted reflections, a relatively large material sample and a much larger number of measurement positions (over 200 positions according to Ref. 6). The authors in the Tamura's paper do not provide any data for the acoustical properties of the

[a]Author to whom correspondence should be addressed. Electronic mail: jprisutova1@sheffield.ac.uk

tested materials below 500 Hz. This enables us to suggest that this method suffers from a typical limitation of those methods which require the compensation for the edge diffraction effect, which, however, depends on the source used.

This paper presents an alternative method for measuring the reflection and absorption coefficient of a relatively large specimen of rigid frame porous media in an acoustic waveguide of square cross-section for which $\lambda \ll d$. The method makes use of the sound pressure and intensity of multimodal field in a waveguide with rigid walls and absorbing termination in the form of a rigidly backed porous material specimen. It is based on one-dimensional Fourier transform which is applied to the sound pressure data recorded with a single microphone roving along the axial direction of the waveguide to simulate a horizontal microphone array. This method can be potentially free from the calibration problems and it is arguably less prone to the influence of the evanescent modes and problems from a poor signal-to-noise ratio caused by standing waves in the pipe. The Johnson–Champoux–Allard equivalent fluid model[7] for the acoustical properties of porous media is used to predict the measured reflection and absorption coefficient spectra for the investigated material specimen. It is found that these spectra are in good agreement with those determined using the standard plane wave impedance tube method[1] and much smaller material specimens.

II. EXPERIMENTAL METHODOLOGY

A. Acoustic setup

The reported experiments were carried out using the large impedance tube facilities available at the Laboratoire d'Acoustique de l'Université du Maine (LAUM). A sketch of an experimental setup is presented in Fig. 1. The impedance tube is a square waveguide constructed from 38 mm thick panels of medium density fiberboard which are varnished to ensure that the walls are perfectly reflective so that they do not contribute noticeably to the level of air attenuation expected for this tube. The absorption of the empty tube was quantified and it does not exceed 15% in the plane wave regime, slightly increasing in the vicinity of the first cut-on frequency. The tube is 4.15 m long and the dimensions of the square cross-section are 300 mm × 300 mm. According to the standard method the high frequency limit for the plane wave regime in this tube was 572 Hz assuming that the sound speed was $c_0 = 343\ \mathrm{ms}^{-1}$ at 20 °C.[1] One end of this tube was terminated with a 30 mm thick aluminum lid, and at the opposite end there were three loudspeakers (S1–S3) which were connected in parallel as shown in Fig. 1. The coordinates of the centers of these three speakers were (50 mm, 50 mm), (50 mm, 150 mm), (150 mm, 150 mm), for speakers S1, S2, and S3, respectively. Such distribution was necessary to increase the number of propagating modes which can be excited in the adopted frequency range of 50 to 1800 Hz. A porous material sample was accurately cut to fit the cross-section of the tube and attached to the metal lid end without an air gap. The signal used for the sound field excitation was a step-by-step sine sweep, ranging from 50 to 1800 Hz, with a step of 12 Hz. A single 1/4 in. B&K microphone was used to avoid problems with phase and amplitude mismatch. This microphone was placed in the corner of the pipe's cross-section, at $x_m = 5$ mm, $y_m = 5$ mm, where the amplitude of all the modes was maximum. The pressure readings were taken at 52 axial positions and the movement of the microphone was controlled by a robotic arm. The first position of the microphone was at the 5 mm distance from the porous material sample, and then the microphone was moved at a 40 mm step, which is consistent with the minimum spacing interval permitted by the Nyquist sampling theorem. This spacing enables us to measure the spatial spectrum with the minimum wavelength of 80 mm. Also, this combination of spacing and maximum adopted frequency allows us to avoid the spatial aliasing problem in frequency-wavenumber space. The data were acquired using a Stanford Research Systems SR785 signal analyzer which enabled us to record the sound pressure signals and store the sound pressure spectra in the text file format. The frequency resolution of this system was 12 Hz. Two materials were studied in this experiment: (a) melamine foam and (b) wood fiber. The material characteristics are discussed in Sec. III.

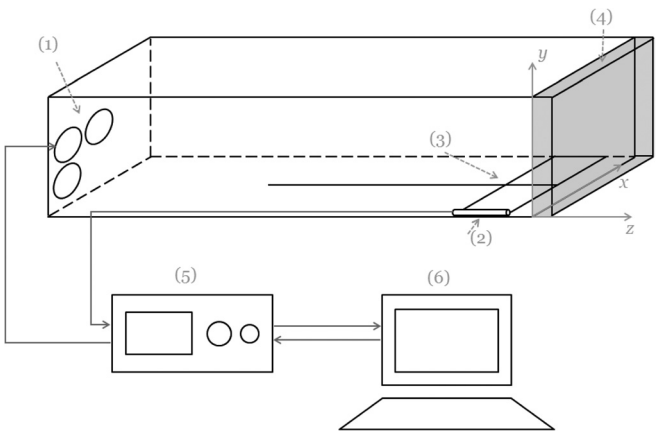

FIG. 1. A schematic illustration of the experimental setup: (1) loudspeakers; (2) microphone; (3) microphone frame designed to maintain the microphone's position in a corner of tube; (4) porous material sample; (5) signal analyzer; (6) PC.

B. Theoretical background

The spatial Fourier transform can be applied to the sound pressure spectra obtained from the described experiments to determine the relations between the wavenumber and frequency spectra (convention $e^{-i\omega t}$). The Fourier integral was applied in the spatial domain and it was approximated with a sum which was taken using the trapezoidal rule, leading to $\tilde{p}_m(K,\omega)$. This trapezoidal rule was applied to the sound pressure data $p_m(z,\omega)$ measured at the $N = 52$ discrete microphone positions:

$$\tilde{p}_m(K,\omega) = \int_{-\infty}^{\infty} p_m(z,\omega) e^{iKz} dz \simeq \frac{\Delta}{2} \sum_{j-1}^{N-1} \left[p_m(z_{j+1},\omega) e^{iKz_{j+1}} + p_m(z_j,\omega) e^{iKz_j} \right], \quad (1)$$

where Δ is the separation between two subsequent microphone positions in the axial direction (i.e., 40 mm), z_j and z_{j+1} are the jth and $(j+1)$th axial positions, respectively.

The sound pressure $p_m(z,\ \omega)$ in a square waveguide (square impedance tube) which is terminated with an absorbing lid (e.g., a rigidly backed porous layer) can be expressed as a superposition of an infinite number of normal modes:

$$p(z,\omega) = \sum_{m=0}^{\infty}\sum_{n=0}^{\infty} \cos\frac{m\pi}{a}x \cos \times \frac{n\pi}{a}y\left(A_{mn}e^{-ik_{mn}z} + A_{mn}R_{mn}e^{ik_{mn}z}\right), \quad (2)$$

where x, y, and z are the coordinates of the microphone, m, n are the indices of the modes propagating in the tube, a is the width of the tube cross-section, k_{mn} is the modal wavenumber, $k_{mn} = \sqrt{k^2 - (m\pi/a)^2 - (n\pi/a)^2}$ with $k = 2\pi\ f/c$, and A_{mn} are the modal excitation coefficient in the incident sound wave and R_{mn} are the unknown modal reflection coefficients which depend on the frequency, on the angle at which the mode is incident on the termination and on the acoustical properties of the porous material from which the specimen at this termination is constructed. The values of the cut-on frequencies for the first few normal modes for the particular impedance tube used in this experiment are presented in Table I (at 20 °C). The Fourier transform of Eq. (2), leading to $\tilde{p}_m(K,\omega)$, is

$$\tilde{p}(K,\omega) = \sum_{m=0}^{\infty}\sum_{n=0}^{\infty} \cos\frac{m\pi}{a}x \cos \times \frac{n\pi}{a}y\left(A_{mn}\int_{-\infty}^{\infty} e^{i(K-k_{mn})z}dz + A_{mn}R_{mn}\int_{-\infty}^{\infty} e^{i(K+k_{mn})z}dz\right). \quad (3)$$

Equation (3) can be analytically simplified by replacing the infinite integration limits with the coordinates of the first and the last microphone measurement positions, z_1 and z_2, to take the following form:

$$\tilde{p}(K,\omega) = \sum_{m=0}^{\infty}\sum_{n=0}^{\infty} \cos\frac{m\pi}{a}x \cos\frac{n\pi}{a}y\left\{A_{mn}\,e^{i(K-k_{mn})(z_2+z_1/2)}(z_2-z_1)\mathrm{sinc}\left[(K-k_{mn})\frac{z_2-z_1}{2}\right] + A_{mn}R_{mn}e^{i(K+k_{mn})(z_2+z_1/2)}(z_2-z_1)\,\mathrm{sinc}\left[(K+k_{mn})\frac{z_2-z_1}{2}\right]\right\}, \quad (4)$$

where sinc $z = \sin z/z$. In Eq. (4) A_{mn} and R_{mn} are the unknowns, which have to be determined for every mode and frequency. For this purpose, the optimization algorithm was applied to the cost function F to minimize the difference:

$$\min_{A_{mn},R_{mn}} F(\omega) = \sum_{K_{\min}}^{K_{\max}} |\tilde{p}_m(K,\omega) - \tilde{p}(K,\omega)|^2 \quad (5)$$

for each of the angular frequencies ω in the measured modal pressure spectra $\tilde{p}_m(K,\omega)$. In the above expression F is the cost function to be minimized, $\tilde{p}(K,\omega)$ is the predicted sound pressure expressed with Eq. (4) and $K_{\min}$ and $K_{\max}$ are the minimum and maximum values of the wavenumber in the wavenumber spectra for which the measured data are available, respectively. These values range from $-25\ \mathrm{m}^{-1}$ to $25\ \mathrm{m}^{-1}$ with the step of $\simeq 0.049\ \mathrm{m}^{-1}$.

It is convenient to express the modal amplitude and the modal reflection coefficient in the following form:

$$A_{mn} = a_{mn}e^{i\phi_{mn}}, \quad A_{mn}R_{mn} = b_{mn}e^{i\psi_{mn}}, \quad (6)$$

where a_{mn}, b_{mn} are the absolute values of the forward and backward waves, i.e., A_{mn} and $A_{mn}R_{mn}$, respectively, whereas ϕ_{mn} and ψ_{mn} are their phases. These quantities are real numbers which are convenient to use in the minimization procedure to estimate the amplitudes and phases in the incident and reflected normal waves. These can then be combined to represent the proportion of the sound energy in the reflected sound wave and the proportion of the sound energy absorbed by the porous specimen through the decomposition of normal waves at a particular frequency. Four examples of the application of the minimization procedure are shown in Fig. 2, presenting the data in two different frequency regimes: plane wave (214 Hz) and fully modal (1236 Hz). These examples are for a 82 mm hard-backed layer of melamine foam. The figures show the amplitudes and phases as functions of the wavenumber before (upper subplots) and after (lower subplots) the application of the minimization procedure. The amplitudes A_{mn} and $A_{mn}R_{mn}$ of the wavenumber in the upper subplots were initially assumed to be equal to 1, and the phases ϕ_{mn} and ψ_{mn}—equal to 0. The results suggest that the minimization procedure enables us to match very closely both the amplitude and the phase of the reflection coefficient below the cut-on frequency with the mean error ε of 1.1% for the amplitude and 1.9% for the phase calculated using

TABLE I. The values of the cut-on frequencies in Hz for a 300 mm square waveguide.

m/n	0	1	2	3
0	0	572	1143	1715
1	572	808	1278	1807
2	1143	1278	1617	2061
3	1715	1807	2061	2425

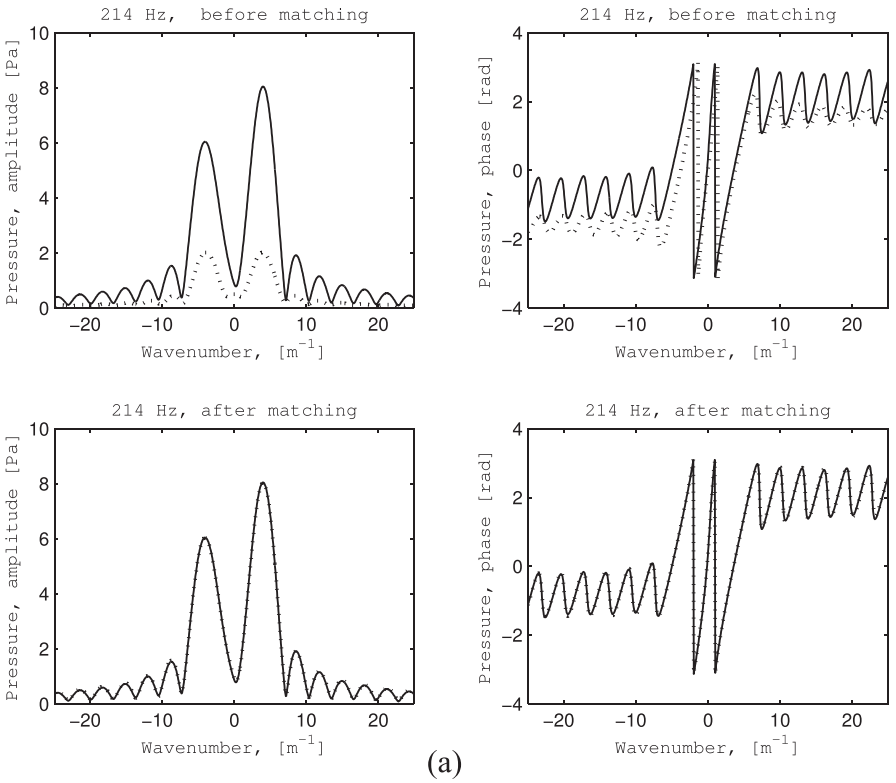

(a)

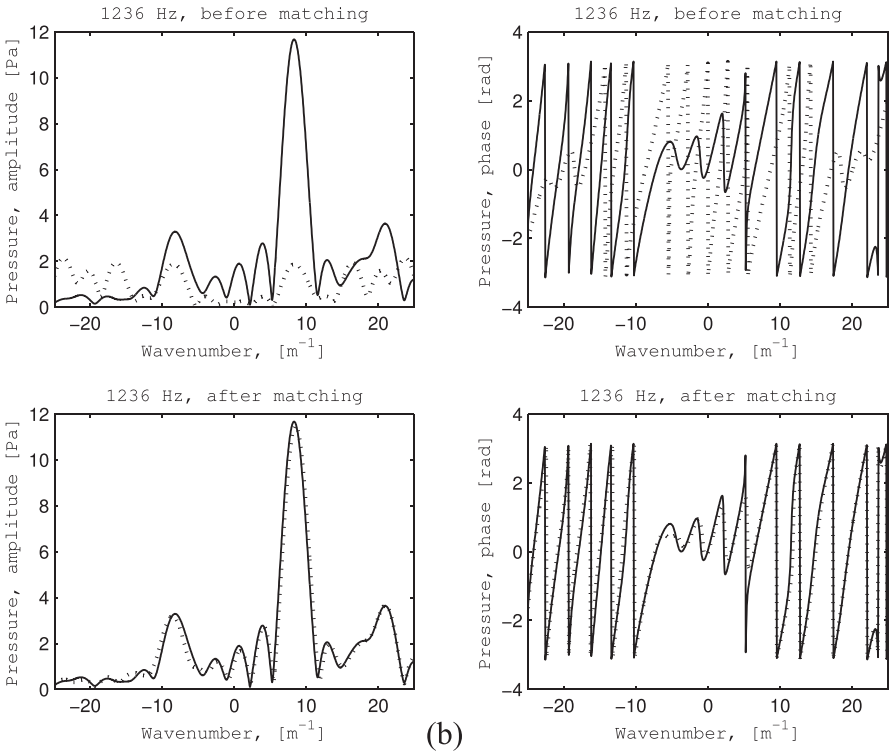

(b)

FIG. 2. The measured and predicted sound pressure amplitude and phase for 214 Hz (a) and 1236 Hz (b) before and after the application of sound pressure matching procedure. Solid line: measured data; dashed line: prediction.

$$\epsilon = \frac{\sum_{w=1}^{N_w} |\tilde{p}_m - \tilde{p}|}{\sum_{w=1}^{N_w} \left| \frac{\tilde{p}_m + \tilde{p}}{2} \right|}. \quad (7)$$

This error can be higher (of the mean value of 5.3% and 23.2%, respectively) when several modes have to be accounted for [see Fig. 2(b)].

The minimization procedure Eq. (5) was applied to recover the absolute values of the modal amplitudes and phases in the considered range of frequencies so that the modal reflection coefficients were determined by the following expression:

$$R_{mn} = \frac{b_{mn} e^{i\psi_{mn}}}{a_{mn} e^{i\phi_{mn}}}. \quad (8)$$

The procedure was performed by making use of MATLAB in-built fminsearch function. It was applied to each mode separately, i.e., the adopted frequency range was divided into several regions, limited by modal cut-on frequencies from each side (50–572 Hz, 572–808 Hz, 808–1143 Hz, 1143–1278 Hz, 1278–1617 Hz, and 1617–1800 Hz). In each region, amplitudes and phases of incident and reflected waves were recovered for each propagating mode, frequency-by-frequency, so for the frequency band of 50–572 Hz amplitudes and phases were recovered for the fundamental mode only, for the frequency band of 572–808 Hz—for the fundamental mode and the first higher mode, etc. The recovered values were imprecise in the vicinity of the cut-on frequencies, but as soon as the frequency of interest was about 40 Hz from the cut-on, the recovered values stabilized.

The absorption coefficient for the plane wave regime, α_{00}, was then calculated in the following standard manner:

$$\alpha_{00} = 1 - |R_{00}|^2. \tag{9}$$

This acoustical quantity does not account for the energy dissipated by the higher order modes. The total absorption coefficient, which does include the energy transmitted by and dissipated through the high order mode absorption mechanisms was calculated using the following expression, which comes from the energy conservation law:

$$\alpha(\omega) = 1 - \frac{\sum_{mn} \frac{\mathrm{Re}(k_{mn})}{\varepsilon_m \varepsilon_n} \|A_{mn} R_{mn}\|^2}{\sum_{m'n'} \frac{\mathrm{Re}(k_{m'n'})}{\varepsilon'_m \varepsilon'_n} \|A_{m'n'}\|^2}, \tag{10}$$

where $\varepsilon_{m\ (m=0)} = 1$ and $\varepsilon_{m\ (m>0)} = 2$. The detailed derivation of this expression is provided in Appendix A.

The angles at which the higher modes impinged on the porous material surface were calculated separately for each mode by making use of the following formula:

$$\theta_{mn}(\omega) = \arccos\left(\frac{\sqrt{\left(\frac{\omega}{c}\right)^2 - \left(\frac{m\pi}{a}\right)^2 - \left(\frac{n\pi}{a}\right)^2}}{\omega/c_0} \right), \tag{11}$$

where m, n are the indices of the modes propagating in the tube.

III. EQUIVALENT FLUID MODEL

It is of direct interest to compare the acoustic reflection and absorption coefficients for the porous materials studied with the proposed experimental method against those obtained from the application of the standard impedance tube method detailed in the ISO 10534-2 standard.[1] It is also of interest to use an equivalent fluid model to predict the observed acoustic behavior of the porous material specimens. For this purpose the experiment with the material samples was carried out in a standard impedance tube which was a circular cross-section metal tube of a 29 mm diameter. The operating frequency range for this tube was 400–6000 Hz. The equivalent fluid model was the Johnson–Champoux–Allard model[7] which enabled us to predict the dynamic density

$$\tilde{\rho}_{\mathrm{eq}}(\omega) = \rho_0 \alpha_\infty \left[1 + \frac{\sigma\phi}{i\alpha_\infty \rho_0 \omega} \left(1 + \frac{4i\alpha_\infty^2 \eta \rho_0 \omega}{\sigma^2 \Lambda^2 \phi^2} \right)^{1/2} \right], \tag{12}$$

and the dynamic bulk modulus

$$\tilde{K}_{\mathrm{eq}}(\omega) = \gamma P_0 \left(\gamma - \frac{(\gamma - 1)}{\left[1 + \frac{\sigma\phi}{i\alpha_\infty \rho_0 N_{Pr} \omega} \left(1 + \frac{4i\alpha_\infty^2 \eta \rho_0 N_{\mathrm{Pr}} \omega}{\sigma^2 \Lambda^2 \phi^2} \right)^{1/2} \right]} \right)^{-1}, \tag{13}$$

where η is the viscosity of air, γ is the specific heat ratio of air, P_0 is the air equilibrium pressure, ρ_0 is the density of air, and N_{Pr} is the Prandtl number.

The following formulas were used for the calculation of the impedance and the modal reflection coefficients at oblique incidence:

$$Z_s(\omega) = -i \frac{Z_c}{\cos\theta_t}(\omega) \cot[k_c(\omega) \cos\theta_t(\omega) d_s], \tag{14}$$

$$Z_c(\omega) = \sqrt{\tilde{\rho}_{\mathrm{eq}}(\omega) \tilde{K}_{\mathrm{eq}}(\omega)}, k_c(\omega) = \omega \sqrt{\frac{\tilde{\rho}_{\mathrm{eq}}(\omega)}{\tilde{K}_{\mathrm{eq}}(\omega)}}, \tag{15}$$

$$R_{mn}(\omega) = \frac{Z_s(\omega)\cos\theta_{mn} - \rho_0 c_0}{Z_s(\omega)\cos\theta_{mn} + \rho_0 c_0}, \tag{16}$$

where

$$\frac{\sin\theta_{mn}(\omega)}{c_0} = \frac{\sin\theta_t(\omega)}{c'(\omega)}, \tag{17}$$

d_s is the material sample thickness, θ_{mn} is the angle of incidence in air, and θ_t and c' are the refraction angle and the speed of sound in porous material. Equation (17) is the classical form of Snell's law of refraction.[8] The non-acoustical parameters used in the above equations are: σ is the flow resistivity, ϕ is the

TABLE II. Characteristics of porous materials.

Parameter	Melamine foam	Wood fiber	Units
Porosity (ϕ)	0.99	0.98	-
Tortuosity (α_∞)	1.01	1.07	-
Flow resistivity (σ)	1.1×10^4	5.0×10^3	Pa s m^{-2}
Viscous characteristic length (Λ)	1.2×10^{-4}	1.0×10^{-4}	m
Thermal characteristic length (Λ')	2.4×10^{-4}	2.0×10^{-4}	m
Layer thickness (d)	0.082	0.095	m

porosity, α_∞ is the tortuosity, Λ is the viscous characteristic length, and Λ' is the thermal characteristic length. The values of these parameters are provided in Table II. These values were obtained using a standard parameter characterization procedure which was carried out by Centre de Transfert de Technologie du Mans (CTTM).

IV. RESULTS AND DISCUSSION

Figures 3 and 4 present the wavenumber-frequency spectra for the sound pressure in the 300 mm × 300 mm impedance tube in the presence of a layer of melamine foam (Fig. 3) and wood fiber (Fig. 4). The data presented in these figures show a clear separation between the first six cross-sectional modes (including the fundamental mode) which are excited in the impedance tube in the frequency range of 50–1800 Hz and at a range of angles of incidence $-\pi/2 < \theta_{mn}(\omega) < +\pi/2$. The waves with positive wavenumbers in Figs. 3 and 4 correspond to those modes which propagate toward the porous layer, whereas the waves with the negative wavenumbers are the modes reflected by the porous layer. This enables us to determine the acoustic reflection coefficient of the porous layer in the frequency range that is much broader than that suggested in the ISO 10534-2 document[1] and for a range of the angle of incidence. This can be achieved using the modal decomposition method and optimization technique detailed in Sec. II. The relationship between the value of the angles $\theta_{mn}(\omega)$, $\theta_t(\omega)$, the frequency $f = \omega/2\pi$ and the modal number is illustrated graphically in Fig. 5 for the case of melamine foam [see Eq. (17)].

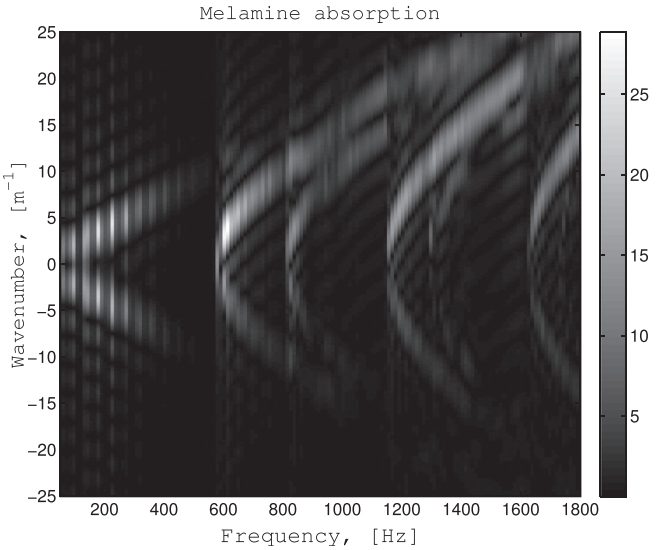

FIG. 3. The wavenumber-frequency spectra (k-ω plot) for the layer of melamine foam.

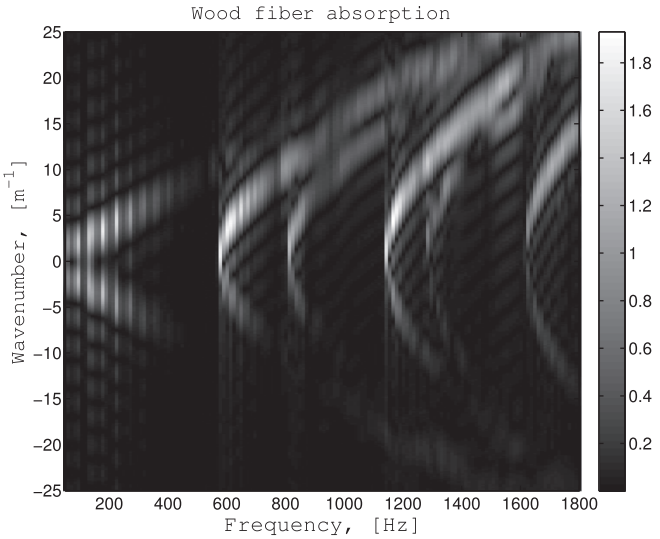

FIG. 4. The wavenumber-frequency spectra (k-ω plot) for the layer of wood fiber.

Figures 6 and 7 show the real and imaginary parts of the modal reflection coefficients as a function of the frequency and the incidence angle which were obtained from the analysis of the wavenumber-frequency spectra for the layer of melamine and wood fiber, respectively. The solid line denotes the experimental data obtained through the application of optimization algorithm Eq. (5), whereas the dashed line is the numerical simulation results obtained using the Johnson–Champoux–Allard equivalent fluid model via expression (16). The experimental data are only provided for those frequencies at which the signal-to-noise ratio was better than 20 dB. For the plane wave regime, the results are presented for the frequency range below the first cut-on frequency at 572 Hz. The differences between the real and imaginary parts of the measured and predicted modal

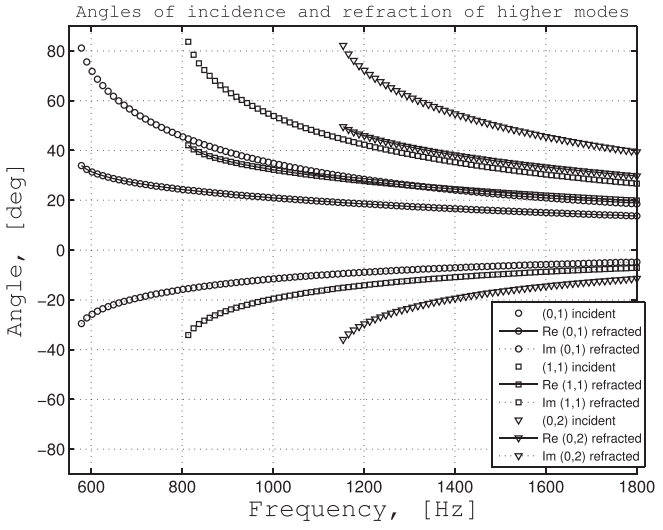

FIG. 5. The mode angle of incidence and real and imaginary parts of the corresponding refraction angle as a function of a frequency for melamine foam.

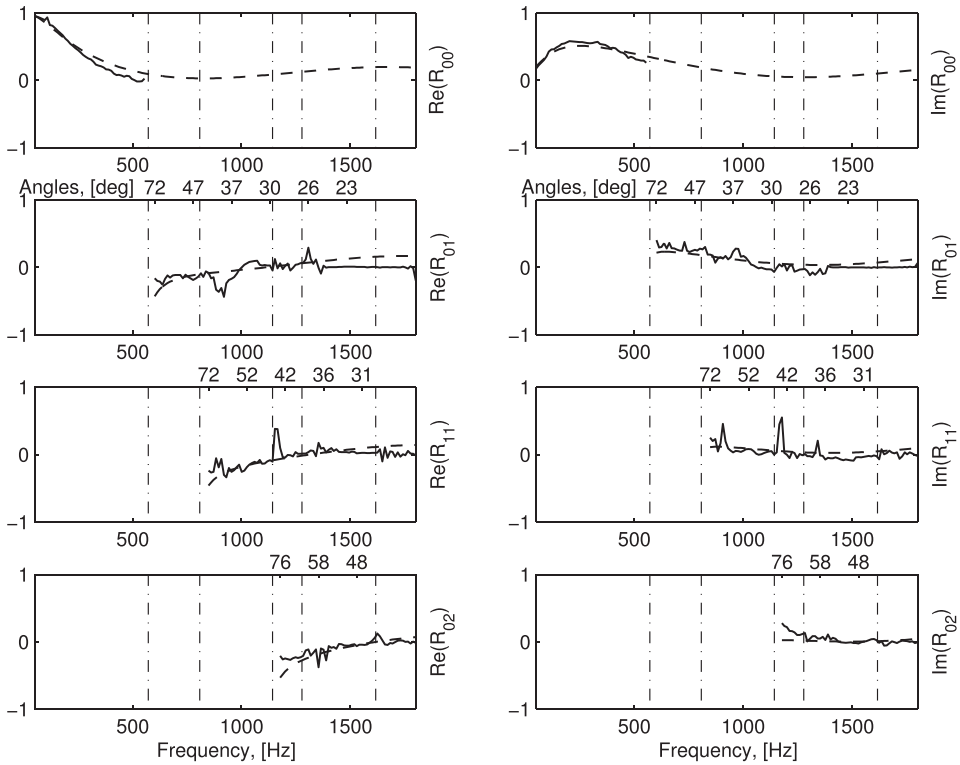

FIG. 6. The measured and predicted modal reflection coefficients for the layer of melamine foam. Solid line: experiments; dashed line: predictions.

reflection coefficients were quantified in terms of the mean difference given by

$$\epsilon_{\mathrm{Re}} = 1/N_q \sum_{q=1}^{N_q} |\mathrm{Re}[R_{mn}^{(\mathrm{m})}(\omega_q) - R_{mn}(\omega_q)]|,$$
$$\epsilon_{\mathrm{Im}} = 1/N_q \sum_{q=1}^{N_q} |\mathrm{Im}[R_{mn}^{(\mathrm{m})}(\omega_q) - R_{mn}(\omega_q)]|, \quad (18)$$

where $R_{mn}^{(\mathrm{m})}(\omega_q)$ is the experimentally determined modal reflection coefficient, $R_{mn}(\omega_q)$ is the predicted reflection coefficient and N_q is the number of frequency points in the reflection coefficient spectrum. These differences are presented in Table III. The differences between the measured and predicted plane wave reflection coefficient are below 0.07. The maximum difference of 0.19 is between the real parts of the measured and predicted reflection coefficient for

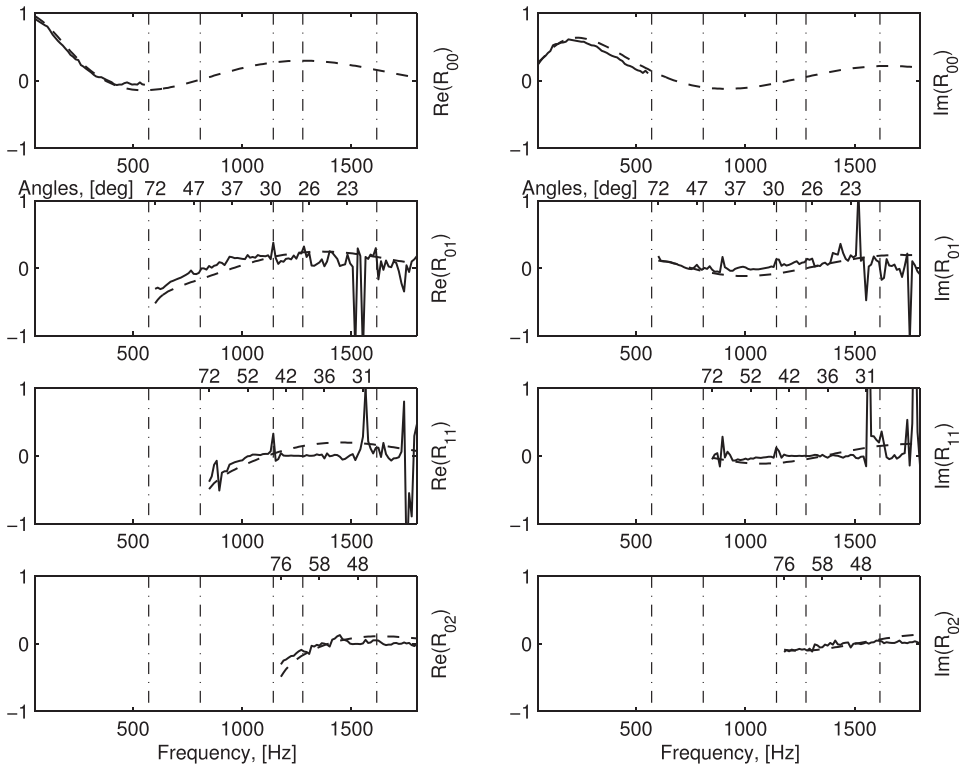

FIG. 7. The measured and predicted modal reflection coefficients for the layer of wood fiber. Solid line: experiments; dashed line: predictions.

TABLE III. A summary of the mean differences between the real and imaginary parts of the measured and predicted modal reflection coefficients for the two material samples.

Mode	Melamine foam		Wood fiber	
	ϵ_{Re}	ϵ_{Im}	ϵ_{Re}	ϵ_{Im}
(0,0)	0.0700	0.0498	0.0427	0.0577
(0,1)	0.136	0.0712	0.1364	0.1174
(1,1)	0.0791	0.0752	0.1857	0.1628
(0,2)	0.0679	0.0514	0.0789	0.0468

mode (11) for the case of wood fiber sample. These errors are attributed to the fact that the measured amplitude of the fundamental mode becomes relatively low above the cut-on frequency of the (01)-mode (572 Hz). A similar effect can be observed in the case of the (11) mode, the amplitude of which becomes relatively low above the cut-on frequency of the (02) mode (1143 Hz). This can be explained by the fact that the adopted speaker arrangement (see Fig. 1) and the cross-sectional position of the microphone array in a corner of the tube favored the excitation of the (01) and (02) modes particularly in the vicinity of their cut-on frequencies. As a result, the signal-to-noise ratio for some modes at some frequencies and angles was limited so that the recovered reflection coefficient data for those modes were less accurate. Evidence from similar experiments conducted in a circular cross-section tube suggests that this phenomenon does not occur at all, or it is much less pronounced when the microphone array is in the middle of the tube.[9] It is also likely that a better speaker arrangement is required to make use of the orthogonality of the mode shapes in the tube so that the mode filtering which is currently attained with Eq. (3) can be enhanced as suggested by Vinogradov and Gavrilov.[10] Another solution is to make use of the orthogonality of normal modes to maximize the excitation coefficients by adopting speakers connected in the form of a phased array.

A common feature between the Figs. 6 and 7 is that the largest discrepancies between the measured and predicted values of the modal reflection coefficients are in the vicinity of the modal cut-on frequencies. Otherwise, the model and measurement agree well and the errors are small. The possible explanation of this is that the integration limits in the Fourier transform analysis were not sufficiently large to capture the modal pressures at or near a cross-sectional resonance. At a cut-on frequency or near it, the modal attenuation is relatively low whereas the modal phase velocity is relatively high so that the adopted spatial length of the fast Fourier transform window in Eq. (1) may not be sufficiently long to capture a representative length of the modal wavefront. The other issue is cross-sectional modes were not properly excited above the frequency of the next cross-sectional resonance. Possible solutions to this issue have already been discussed in the previous paragraph.

Figures 8 and 9 present the total absorption coefficient spectra in the frequency range of 50–1800 Hz. The experimental and theoretical values of the total absorption coefficient were calculated from Eq. (10) using the measured and predicted sound pressure level spectra, respectively. The discrepancy between the measured and predicted absorption coefficient was quantified in terms of the relative error in a way similar to that described by Eq. (7). The error between the experimental and predicted total absorption coefficient is equal to 3.7% in case of the melamine foam and it is 3.3% in case of the wood fiber. These figures also show the theoretical and experimental values of the plane wave absorption coefficient, which were calculated using the sound pressure data obtained in the 29 mm impedance tube in accordance

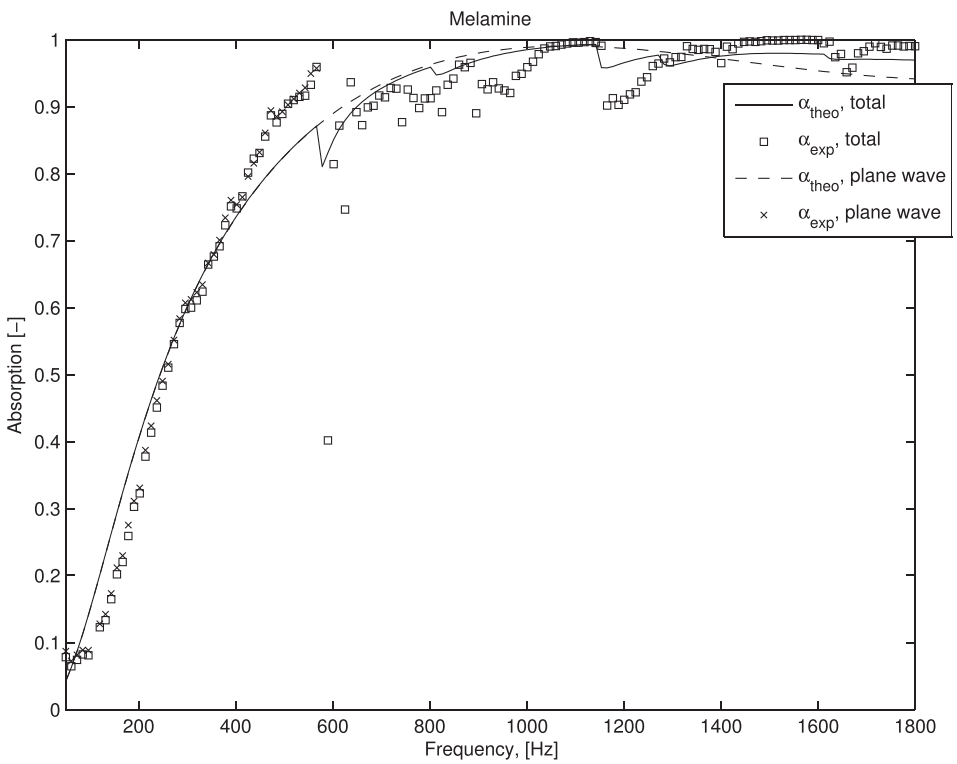

FIG. 8. The measured and predicted absorption coefficient spectra for melamine foam. Black squares: experimental total absorption coefficient; solid black line: predicted total absorption coefficient; black asterisks: experimental plane wave absorption coefficient; dashed black line: predicted plane wave absorption coefficient.

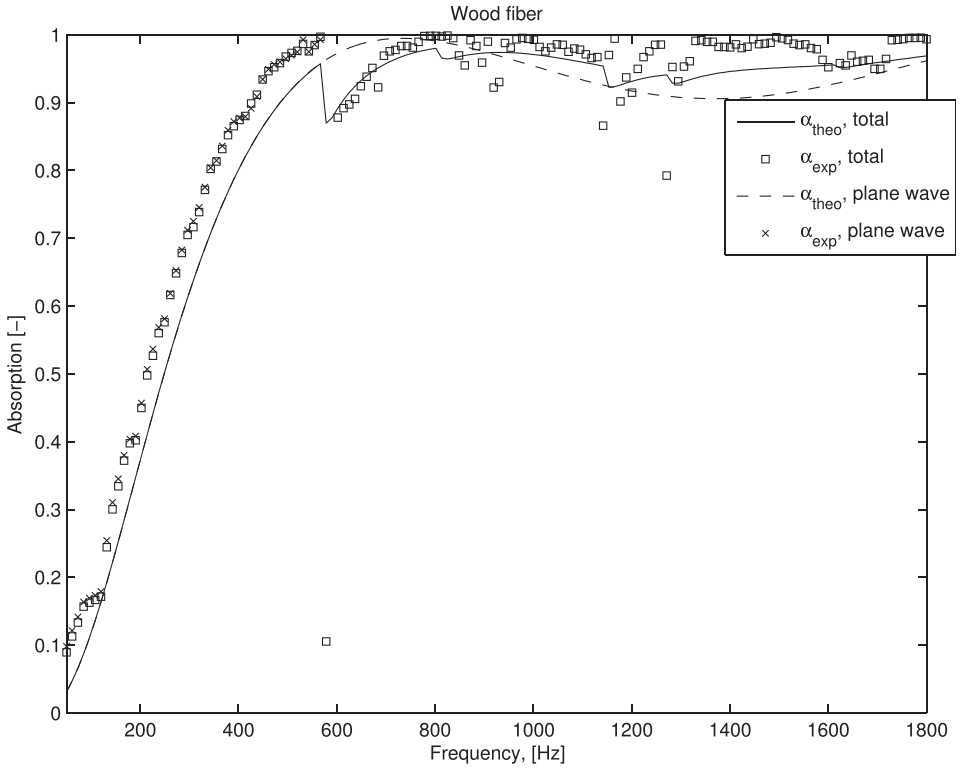

FIG. 9. The measured and predicted absorption coefficient spectra for wood fiber. Black squares: experimental total absorption coefficient; solid black line: predicted total absorption coefficient; black asterisks: experimental plane wave absorption coefficient; dashed black line: predicted plane wave absorption coefficient.

with the ISO 10534-2 procedure[1] and predicted using Eqs. (9), (16), and the non-acoustical parameters listed in Table II. The error between the measured total absorption coefficient [Eq. (10)] and measured plane wave absorption coefficient [Eq. (9)] for an entire frequency range is 3.2% for the melamine foam and 5.1% for the wood fiber. However, one should not expect a full agreement between these two cases, as absorption in the 29 mm and 300 mm impedance tubes is not the same beyond the first cut-on frequency of the latter.

The match between the predicted and measured total absorption coefficient data is remarkably close until the first cut-on frequency of 572 Hz. At the first cut-on frequency there is a sharp decrease in the experimental absorption coefficient for both melamine foam and wood fiber which is partly matched by the predicted data. This decrease takes place each time when the frequency of sound approaches a cross-sectional resonance when the incident angle for the normal mode becomes large. In the case of melamine foam the predicted data match better the behavior of the measured total absorption coefficient between the resonances than near these resonances. For this material, the total absorption coefficient appears to fluctuate about the spectrum of the normal incidence, plane wave absorption coefficient. In the case of wood fiber, the predicted total absorption coefficient spectrum agrees better with the measured data across the whole frequency range than it does in the case of melamine foam. The total absorption coefficient for wood fiber material appears 5%–10% higher than the normal incidence, plane wave absorption coefficient for this material. It appears that in case of the higher order modes the measured data fluctuate between the normal incidence and diffused field absorption coefficient, matching the diffused field absorption coefficient at the cut-on frequencies. Another thing which can be remarked is that for both materials the amplitude of the experimental absorption coefficient is higher than of the predicted. It can be attributed to the fact that the walls of the waveguide are not perfectly reflecting and partially absorb sound.

V. CONCLUSIONS

This paper presents a new method to measure the reflection and absorption coefficients of a porous layer in an impedance tube which lateral dimensions are larger than the acoustic wavelength. The proposed method is based on measuring the sound pressure spectra with a horizontal microphone array and then applying the spatial Fourier transform to these data to separate the incident modal field from the modal field reflected from the porous layer. It has been shown that in this way the high frequency limit of a rectangular impedance tube can be extended at least by a factor of three. This enables us to measure the acoustical properties of much larger material specimens well beyond the high frequency limit that is currently set in the standard.[1] A most attractive feature of this method is that it yields both frequency and angular dependent complex reflection coefficient data for a porous layer. This enables us to measure in the laboratory the acoustical properties of a large porous specimen at a range of the angles of incidence and in a relatively wide frequency band. Unlike other methods based on multiple sound pressure readings which are subsequently used in the spatial Fourier transform,[6] the proposed method does not require the compensation for the edge diffraction effect because of the sample being present in a bounded waveguide with acoustically hard walls. This enables us to measure reliably the acoustical properties of large material specimens in the low frequency end (50 Hz in the presented work). Furthermore, the proposed experimental setup is rather time-efficient and easy to run and it does not require

large material specimen. The reason for choosing the high frequency end equal to 1800 Hz was the balance between the measurement time, the number of measurement points per wavelength and maximum frequency in the reflection coefficient spectra to which the standard method can be extended. The wavelength of the plane wave at 1800 Hz is $\lambda = 188$ mm at $T = 20\,^{\circ}$C. The step between the measurement positions is 40 mm which is just under $\lambda/5$. Increasing this limit further will require a proportionate reduction in the spatial step to ensure that integral (1) is accurately evaluated. This will result in the proportionate increase in the duration of the experiment leading to measurements taking excessive amount of time.

The proposed method has been used to obtain the complex reflection coefficient and absorption coefficient spectra for a layer of melamine foam and wood fiber. These materials have been characterized independently to derive the values of non-acoustical parameters so that the Johnson–Champoux–Allard equivalent fluid model[7] could be used to predict the complex modal reflection coefficient and absorption coefficient spectra for these two types of materials. It has been shown that a good match between the measured and predicted modal reflection coefficients across the whole frequency range can be achieved using an optimization analysis whereby the difference between the measured and predicted spatial sound pressure spectra is minimized for a given frequency of sound. The measured and predicted modal reflection coefficient frequency spectra agree within 5%–15%, whereas the absorption coefficient spectra agree within 5%. The agreement between the absorption coefficient spectra measured using the proposed measurement method and the normal incidence, plane wave absorption coefficient spectra measured in the 29 mm impedance tube is within 5%–10% across the whole frequency range. However, it is not possible to achieve a total agreement between these two cases at frequencies higher than the first cut-on frequency of the 300 mm impedance tube, as beyond it the measurements are not equal. The agreement between the measured and predicted absorption coefficient spectra is particularly close in the plane wave regime below the frequency of the first cross-sectional resonance. However, in the vicinity of a cross-sectional resonance this agreement can deteriorate, making the results imprecise. This happens due to some cross-sectional modes beginning to dominate whereas the others are not excited strongly enough to be resolved with the proposed modal analysis method. A poor signal-to-noise ratio affects the accuracy with which the modal reflection coefficients can be derived using the optimization algorithm. This issue can be addressed by either adopting a phased speaker array or by repeating the measurements with the same microphone array moved to an alternative cross-sectional position in the impedance tube. The influence of the microphone at high frequencies has been neglected, as well as the absorption of the tube, which might have contributed to the discrepancies between the experimental results and the predictions in higher frequency range. The ability to excite a sufficient number of modes and to capture these modes accurately by positioning the microphone at those locations where the modal amplitude is much higher than that of the background noise can pose a challenge as well. Finally, measuring at a sufficient number of points to be able to apply accurately the spatial discrete Fourier transform can limit the quality of the recovered data.

APPENDIX A: THE TOTAL ABSORPTION COEFFICIENT OF AN ABSORBING TERMINATION IN A MULTI-MODAL WAVEGUIDE

Equation (10) can be derived from the basic knowledge of the energy relations in a waveguide. Equation (2) suggests that the modal decomposition of the sound field in the impedance tube combines two groups of waves: those which are incident on the material specimen (t being the time)

$$p_{mn}^{(i)}(x,y,z,t) = \cos\frac{m\pi}{a}x\cos\frac{n\pi}{a}yA_{mn}e^{-ik_{mn}z+i\omega t}; \tag{A1}$$

and those which are reflected from it

$$p_{mn}^{(r)}(x,y,z,t) = \cos\frac{m\pi}{a}x\cos\frac{n\pi}{a}yA_{mn}R_{mn}e^{ik_{mn}z+i\omega t}. \tag{A2}$$

The difference between these two groups is in the sign in the exponential function $e^{\pm ik_{mn}z}$ and in the presence of the reflection coefficient term in Eq. (A2). The z-component of the intensity vector in a propagating normal wave is a measure of energy which this wave carries from the source toward the material sample. This instantaneous intensity is the product of the sound pressure $I_{mn} = \mathrm{Re}\{p_{mn}^{(i)}v_{mn}\}$. The z-component of the acoustic velocity vector of the mode (mn) is given by

$$v_{mn} = \frac{1}{i\omega\rho}\frac{\partial p_{mn}^{(i)}}{\partial z} = \frac{k_{mn}p_{mn}^{(i)}}{\omega\rho}, \tag{A3}$$

and this suggests that

$$I_{mn}(x,y,x,t) = \frac{k_{mn}A_{mn}^2}{\omega\rho}\cos^2(\xi_m x)\cos^2(\xi_n y)\cos^2(-k_{mn}z+\omega t), \tag{A4}$$

with $\xi_m = m\pi/a$. The time-averaged intensity is

$$\tilde{I}_{mn}(x,y) = \frac{\mathrm{Re}(k_{mn})A_{mn}^2}{2\omega\rho}\cos^2(\xi_m x)\cos^2(\xi_n y). \tag{A5}$$

The mode (mn) incident on the material surface carries the energy flux through the cross-section of the impedance tube ($S = a^2$) which is the integral of Eq. (A5), i.e.,

$$E_{mn} = \int_S \tilde{I}_{mn}(x,y)dS = \int_0^a\int_0^a \tilde{I}_{mn}(x,y)dxdy, \tag{A6}$$

where a is the dimension of the side of the square cross-section of the impedance tube S. It is easy to show that the integration of Eq. (A6) with respect to x and y gives the following expression for the total energy flux in the normal mode (mn) incident on the material specimen

$$E_{mn}^{(i)} = \frac{\mathrm{Re}(k_{mn})A_{mn}^2}{2\varepsilon_m\varepsilon_n\omega\rho}, \tag{A7}$$

where $\varepsilon_{m\ (m=0)} = 1$ and $\varepsilon_{m\ (m>0)} = 2$ are the same as those defined in Eq. (10). The wavenumber k_{mn} here is considered to be real because evanescent modes do not carry the energy.

The above arithmetical manipulations can be used to derive the total energy flux in the mode (mn) reflected from the material specimen and it is easy to show that

$$E_{mn}^{(r)} = \frac{\mathrm{Re}(k_{mn})\|A_{mn}R_{mn}\|^2}{2\varepsilon_m\varepsilon_n\omega\rho}, \tag{A8}$$

where the norm $\|A_{mn}R_{mn}\|$ is applied because the quantity $A_{mn}R_{mn}$ which contains the modal reflection coefficient R_{mn} is no longer real.

The total energy flux is the sum of the energies in all of the propagating modes, therefore

$$E^{(i)} = \sum_{mn} \frac{\mathrm{Re}(k_{mn})A_{mn}^2}{2\varepsilon_m\varepsilon_n\omega\rho}, \tag{A9}$$

and

$$E^{(r)} = \sum_{m'n'} \frac{\mathrm{Re}(k_{m'n'})\|A_{m'n'}R_{m'n'}\|^2}{2\varepsilon_{m'}\varepsilon_{n'}\omega\rho}. \tag{A10}$$

By its definition, the absorption coefficient is the ratio of the energy absorbed by the surface $(E^{(i)} - E^{(r)})$ to the incident sound energy $(E^{(i)})$, i.e., $\alpha = (E^{(i)} - E^{(r)})/E^{(i)}$. Making use of this definition and Eqs. (A9) and (A10) yields

$$\alpha(\omega) = 1 - \frac{\sum_{m'n'} \frac{\mathrm{Re}(k_{m'n'})\|A_{m'n'}R_{m'n'}\|^2}{\varepsilon_{m'}\varepsilon_{n'}}}{\sum_{mn} \frac{\mathrm{Re}(k_{mn})A_{mn}^2}{\varepsilon_m\varepsilon_n}}, \tag{A11}$$

which is the equation identical to Eq. (10) defined at the end of Sec. II B.

APPENDIX B: SENSITIVITY ANALYSIS

In order to estimate what influence measurement errors may have on the measured modal reflection coefficients, a sensitivity analysis was carried out. The Johnson–Champoux–Allard equivalent fluid model[7] was used to predict the modal reflection coefficients which were then substituted in the equation for the frequency spectrum of the sound pressure [see Eq. (2)] in which measurement errors, $e(\omega)$, were artificially added, i.e., $p_e(z, \omega) = p(z, \omega) + e(\omega)$. The simulated sound pressure with errors, $p_e(z, \omega)$, was then used to calculate the spatial Fourier transform, $\tilde{p}_e(K, \omega)$, in accordance to Eq. (1). The simulated spatial spectra, $\tilde{p}_e(K, \omega)$, were then used in the optimization analysis [see Eq. (5)] instead of the measured sound pressure, $\tilde{p}_m(K, \omega)$, to

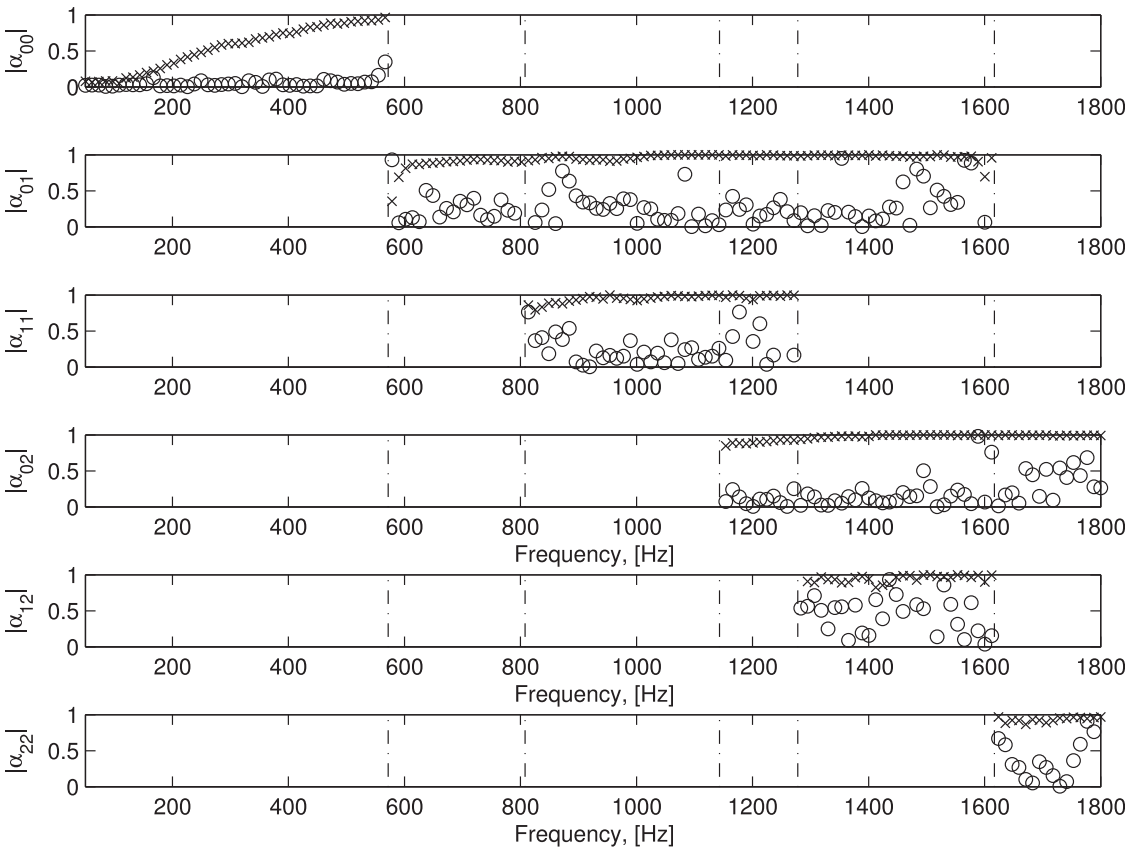

FIG. 10. The partial absorption coefficients for the empty tube (circles) and for melamine foam (crosses).

study how the artificially added errors affect the ability of the proposed measurement method to measure the modal reflection coefficients, R_{mn}.

Three types of error were considered in this analysis: (i) a random error in the sound pressure phase spectrum within $\pm 20\%$; (ii) a random ± 10 mm positioning error applied separately to the sound pressure at each of the 52 microphone positions; and (iii) a constant 10 mm bias in positioning applied to the whole microphone array. The mean difference between the modal reflection coefficient computed exactly for the 52 microphone positions as assumed in Sec. II B and the simulated one containing the added error was then determined. This difference was quantified for the real and imaginary parts of the reflection coefficient according to the following expressions:

$$\epsilon_{Re} = \frac{1}{N}\sum_{n=1}^{N} |\mathrm{Re}[R_{mn}^{\mathrm{pred}}(\omega_n)] - \mathrm{Re}[R_{mn}^{\mathrm{sim}}(\omega_n)]|,$$
$$\epsilon_{\mathrm{Im}} = \frac{1}{N}\sum_{n=1}^{N} |\mathrm{Im}[R_{mn}^{\mathrm{pred}}(\omega_n)] - \mathrm{Im}[R_{mn}^{\mathrm{sim}}(\omega_n)]|, \quad \text{(B1)}$$

where R_{mn}^{pred} is the frequency-dependent reflection coefficient calculated exactly, and R_{mn}^{sim} is the frequency-dependent reflection coefficient with simulated error.

The results suggest that the $\pm 20\%$ uncertainty in the measured phase results in the 0.0280 maximum difference between the exact value of the modal reflection coefficient and its simulated counterpart, which is approximately 2.5 times less than the experimentally found difference (see Table III). A 10 mm misalignment in any of the 52 the microphone positions results in the maximum difference of 0.0268, which is approximately five times less than the experimentally found difference. The constant axial bias introduced to the microphone array as a whole results in the maximum difference of 0.0382, which is approximately two times less that the experimentally found difference. These differences are not enough to explain the observed mismatch between the predicted modal reflection coefficients and the measured data. The measured reflection coefficient seems to exhibit a greater sensitivity to other factors which may influence the accuracy of the collected data. One of such factors may be the residual absorption of the impedance tube. In Fig. 10, the partial absorption coefficients of an empty tube (marked with circles) are compared to those of melamine foam (marked with crosses). Although the empty tube absorption is relatively small in comparison to melamine foam and on average does not exceed 15%, there are certain frequencies at which the residual absorption is relatively high and can be of the same magnitude as the material's absorption. This places a restriction on the accuracy of the absorption coefficient data which can be measured with the proposed method in this particular impedance tube.

[1]ISO 10534-2:1998, Determination of sound absorption coefficient and impedance in impedance tubes, Part 2: Transfer-function method (International Organization for Standardization, Geneva, Switzerland 1998).
[2]J.-M. Coulon, F. Chevillotte, F.-X. Bécot, and L. Jaouen, "Broadband acoustical characterisation in a horn shaped impedance tube," *Proc. Acoustics* 2012, Nantes, France, pp. 1903–1907, CD-ROM.
[3]M. Akoum and J.-M. Ville, "Measurement of the reflection matrix of a discontinuity in a duct," J. Acoust. Soc. Am. **103**(5), 2463–2468 (1998).
[4]T. Schultz, L. N. Cattafesta III, and M. Sheplak, "Modal decomposition method for acoustic impedance testing in square ducts," J. Acoust. Soc. Am. **120**(6), 3750–3757 (2006).
[5]M. Tamura, "Spatial Fourier transform method of measuring reflection coefficients at oblique incidence. I: Theory and numerical examples," J. Acoust. Soc. Am. **88**(5), 2259–2264 (1990).
[6]M. Tamura, J.-F. Allard, and D. Lafarge, "Spatial Fourier transform method of measuring reflection coefficients at oblique incidence. II. Experimental results," J. Acoust. Soc. Am. **97**(4), 2255–2262 (1995).
[7]Y. Champoux and J.-F. Allard, "Dynamic tortuosity and bulk modulus in air–saturated porous media," J. Appl. Phys. **70**(4), 1975–1978 (1991).
[8]J.-F. Allard and N. Attala, *Propagation of Sound in Porous Media: Modelling Sound Absorbing Materials* (Wiley, Chichester, UK, 2009), Chap. 3.
[9]J. Prisutova, "Acoustic intensity in waveguides," MPhil to Ph.D. transfer report, University of Bradford, 2012.
[10]M. S. Vinogradov and A. N. Gavrilov, "Cross-correlation of normal modes in a shallow sea," Sov. Phys.–Acoust. **33**, 241–243 (1987).